PERGAMON

International Journal of Heat and Mass Transfer 42 (1999) 1353–1362

International Journal of HEAT and MASS TRANSFER

The Sparrow–Galerkin solution of radiation exchange and transition to finite element

W.J. Minkowycz[a], A. Haji-Sheikh[b,*]

[a] *Department of Mechanical Engineering, University of Illinois at Chicago, Chicago, IL 60607-7022, U.S.A.*
[b] *The University of Texas at Arlington, Arlington, TX 76019-0023, U.S.A.*

Received 16 April 1998; in final form 13 August 1998

Abstract

This paper presents a historical perspective on the development of the Galerkin-type and finite-element calculations of radiation exchange between surfaces. It is shown that the formulation of the variational solution of radiation exchange introduced by Sparrow in the 1950s is similar to that used by Galerkin to solve differential equations. The extension of Galerkin's method to the integral equations of the Fredholm type yields the formulations developed by Sparrow using the variational method. For this reason, the Galerkin-type solutions of radiation exchange will be referred to as the Sparrow–Galerkin method. The Sparrow–Galerkin solution technique, in most cases, provides highly accurate results. However, for a certain set of parameters, the series solutions may not converge. This leads to formulation of a finite-element technique as the discretized form of the Sparrow–Galerkin method evolves into the finite-element method.

Nomenclature

$a^{k,j}_{m,m}$ members of matrix $\mathbf{A}^{k,j}$
A area [m^2]
$\mathbf{A}$ matrix of coefficient
$\mathbf{A}^{k,j}$ square matrices in matrix $\mathbf{A}$
B radiosity [W m^{-2}]
d_m coefficients
$\mathbf{d}$ array of coefficients
f_m basis functions
h gap dimension [m]
H irradiation [W m^{-2}]
I variational function
K_{ij} kernel function
L plate dimension [m]
i, j, k indices
$\boldsymbol{i}, \boldsymbol{j}, \boldsymbol{k}$ unit vectors along x, y, z
l, m, n indices
m_k index
M number of functions
$\boldsymbol{n}$ unit normal vector
N number of surfaces
r radial coordinate [m]
r_{ij} local distance between A_i and A_j
$\boldsymbol{r}$ unit vector along r_{ij}
T temperature [K]
x, y, z coordinates [m].

Greek symbols

β angle between radiation incident and $\boldsymbol{n}$
δ vector along element boundary
ε emittance
ζ local coordinate [m]
η variational function, equation (6)
λ parameter in equations (4) and (9)
ξ local coordinate [m]
ρ reflectance
σ Stefan–Boltzmann coefficient [W m$^{-2}\cdot$K^{-4}]
ϕ variational function
χ unknown function in equations (4) and (9)
$\boldsymbol{\chi}$ vector of χ values in finite element
ψ known function in equations (4) and (9)
ω variational parameter, see equation (11).

* Corresponding author. Tel.: 001 817 272 2010; fax: 001 817 272 2952; e-mail: haji@mae.uta.edu

0017–9310/98/$ - see front matter
PII: S0017–9310(98)00271–3

1. Introduction

The governing equations for radiation exchange between surfaces are integral equations of the Fredholm type. In the 1950's, Sparrow [1] introduced a variational method to solve radiation exchange problems. Recently, it is common to extend the Galerkin method developed for solving differential equations [2] to radiation exchange integral equations. The Galerkin solution in a discretized form is generally referred to as the finite-element method. The extension of the Galerkin method to radiation exchange problems yields exactly the same formulation that Sparrow introduced in the 1950's using the Ritz variational method [1, 3]. This fact is not clearly stated in the literature.

Finite element is a powerful numerical technique that can handle a broad range of heat transfer problems, It is widely used in conductive, convective, and radiative applications. In particular, finite element has become a popular tool when dealing with radiation in a participating media. Recent finite element work in thermal radiation, reported in the literature, is numerous; therefore, this work contains only a brief survey of pertinent literature. A comprehensive discussion of the finite-element method (FEM) and application to conducting bodies with radiating surfaces is in Huebner et al. [4]. An adaptive FEM modeling of radiative heat transfer coupled with conduction is given by Daurelle et al. [5]. Lobo and Emery [6, 7] analyzed combined conduction and radiation in nonparticipating media and they show anomalous FEM solution behaviour when the radiation component dominates the conduction components. They showed that using higher-order basis functions can alleviate this problem. Kuppurao and Derby [8] studied the FEM solution of radiant interchange among diffuse-gray surfaces using a higher-order-accurate view factor that depends on geometry. Finite element formulation, in particular, the discrete ordinate method, for application to absorbing, emitting, and scattering media is reported by Sanchez and Smith [9], Fiveland [10], Fiveland and Jessee [11], and others [12, 13].

The variational formulations of Sparrow [1, 3] are exactly the same as the finite element formulations based on the weighted residuals. Accordingly, it is appropriate to review the work done by Sparrow [1, 3] as a prelude to the formulation of the finite-element method.

1.1. Sparrow variational equation

At the outset, formulation of the radiation exchange problems will be limited to a simple case discussed by Sparrow [1]. The configuration consists of two parallel plates a distance h apart, Fig. 1. The plates have a dimension L in the x-direction and are infinitely long perpendicular to the plane perpendicular to the x-axis. The

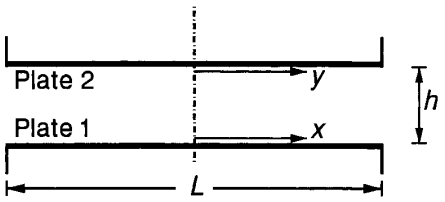

Fig. 1. Schematic of two parallel plates.

plates are at the same temperature and have equal emissivities. The radiosity is defined by equation

$$B(x) = \varepsilon\sigma T^4 + \rho H(x) \tag{1}$$

where $H(x)$ is known as the irradiation to the surface. The radiosity for diffusely emitting and diffusely reflecting surfaces is governed by equation (1)

$$B(x) = \varepsilon\sigma T^4 + \frac{\rho h^2}{2}\int_{-L/2}^{L/2} \frac{B(y)\,\mathrm{d}y}{[(y-x)^2+h^2]^{3/2}} \tag{2}$$

where y is a dummy variable of integration. The value $H(x)$ in equation (1) is replaced by

$$H(x) = \frac{h^2}{2}\int_{-L/2}^{L/2} \frac{B(y)\,\mathrm{d}y}{[(y-x)^2+h^2]^{3/2}} \tag{3}$$

to yield equation (2). Equation (2) has a form commonly referred to as the Fredholm integral equation. For the sake of brevity, it is written as

$$\chi(x) = \psi(x) + \lambda\int_a^b \chi(y)K(x,y)\,\mathrm{d}y. \tag{4}$$

Sparrow [1] introduced the following variational expression for the functional I to be minimized,

$$I = \int_a^b [\chi(x)]^2\,\mathrm{d}x - 2\int_a^b \chi(x)\psi(x)\,\mathrm{d}x - \lambda\int_a^b\int_a^b \chi(x)\chi(y)K(x,y)\,\mathrm{d}y\,\mathrm{d}x. \tag{5}$$

For convenience of this presentation, the functional I in equation (5) is the negative of that in ref. [1]. This minor modification causes the extremum of equation (5) to become a minimum. Equation (5), using minimization principles, yields equation (4). For the purpose of proof, the function that will minimize I is designated as $\bar{\chi}$, so that

$$\chi(x) = \bar{\chi}(x) + \omega\eta(x) \tag{6a}$$

$$\chi(y) = \bar{\chi}(y) + \omega\eta(y) \tag{6b}$$

where ω is the variational parameter and η is an arbitrarily selected function. After substituting $\chi(x)$ and $\chi(y)$ in equation (5), the functional I can be minimized. This is accomplished by setting $\partial I/\partial\omega = 0$. Of course, the function $\bar{\chi}(x)$, calculated to minimize I, approaches the solu-

tion function $\chi(x)$ when $\omega \to 0$. Following the minimization principle [1], equation (5) becomes

$$\left(\frac{\partial I}{\partial \omega}\right)_{\omega=0} = 2\int_a^b \eta(x)\left[\chi(x) - \psi(x) - \int_a^b \chi(y)K(x,y)\,\mathrm{d}y\right]\mathrm{d}x = 0. \quad (7)$$

This relation is valid for all values of $\eta(x)$; therefore, the term in the square brackets is equal to zero. Equation (7) also describes a technique commonly known as the method of weighted residuals. Accordingly, the minimization of I led to equation (4). For I to be a minimum, the second derivative of I with respect to ω must be unconditionally positive. This will be demonstrated later.

Sparrow [1] replaced χ by a linear combination of a complete set of independent functions,

$$\chi(x) = \sum_{m=1}^{M} d_m f_m(x). \quad (8)$$

In the Sparrow formulation, $f_m(x) = x^{2(m-1)}$ represents the basis functions and $\eta(x)$ in equation (7) becomes the basis function $f_m(x)$ for $m = 1, 2, 3, M$. Specifically, Sparrow [1] considered $\chi(x) = d_1 + d_2x^2 + d_3x^4$ and substituted for $\chi(x)$ and $\chi(y)$ in equation (7). This makes I a function of d_1, d_2, and d_3. Setting $\partial I/\partial d_1 = 0$, $\partial I/\partial d_2 = 0$, and $\partial I/\partial d_3 = 0$, leads to three linear equations. The basic steps are described in ref. [1].

In a numerical example, Sparrow [1] demonstrated that high accuracy is achievable using the methodology described above. For the configuration in Fig. 1, the worst accuracy is reported [1] when both h/L and the emissivity are small. For instance, in the dimensionless form, for $h/L = 0.1$ and $\varepsilon = 0.1$, Sparrow calculated $\chi(x) = B(x)/\varepsilon\sigma T^4$ as

$$\chi(x) = 7.205 - 10.06x^2 - 27.81x^4; \quad \text{for } -0.5 \leqslant x \leqslant 0.5.$$

It is shown that at $x = \pm 0.5$, the error is less than 2%. Generally, an accurate solution is possible when polynomials are of degrees 6–8.

The procedure developed by Sparrow [1] is exactly the same as the extension of the weighted residuals method [2] to the Fredholm integral equation. In the method of weighted residuals, both sides of the energy transport equation, equation (4), are multiplied by a basis function, $f_m(x)$, then integrated over the domain of $\chi(x)$. Both procedures produce exactly the same relation, specifically, equation (7). Galerkin introduced the method of weighted residuals to solve differential equations [2] while Sparrow developed this methodology to evaluate radiation interchange among surfaces; hence, the methodology is called Sparrow–Galerkin. The use of equation (7) instead of equation (5) simplifies the procedure without changing the formulations or results. In other words, the Sparrow–Galerkin procedure is a shortcut that bypasses the mathematical steps of variational calculus. Following this introduction, the generalized formulation of the Sparrow–Galerkin method and its transition to the finite-element method is presented.

2. Generalized variational formulation

The method described above is for a simple problem. The radiation exchange usually takes place between many surfaces with different temperatures and surface properties. Sparrow and Haji-Sheikh [3] presented a generalized variational principle for multisurface applications. A brief mathematical formulation is described below; the complete derivations are available in ref. [3]. The radiation exchange between surfaces is given by the relation

$$\chi_i(\boldsymbol{r}_i) = \psi_i(\boldsymbol{r}_i) + \lambda_i \sum_{j=1}^{N} \int_{A_j} \chi_j(\boldsymbol{r}_j)K_{ij}(\boldsymbol{r}_i, \boldsymbol{r}_j)\,\mathrm{d}A_j; \quad \text{for } i = 1, 2, \ldots, N \quad (9)$$

where $\boldsymbol{r}_i$ and $\boldsymbol{r}_j$ are the position vectors for surfaces i and j. The function $K_{ij}(\boldsymbol{r}_i, \boldsymbol{r}_j)$ is related to the angle factor of configuration factor, $\mathrm{d}F_{ij} = K_{ij}(\boldsymbol{r}_i, \boldsymbol{r}_j)\,\mathrm{d}A_j$. The reciprocity relation shows that $K_{ij} = K_{ji}$. The generalized variational relation is

$$I = \sum_{i=1}^{N} \frac{1}{\lambda_i} \int_{A_i} [\chi_i(\boldsymbol{r}_i)]^2\,\mathrm{d}A_i - 2\sum_{i=1}^{N} \frac{1}{\lambda_i} \int_{A_i} \chi_i(\boldsymbol{r}_i)\psi_i(\boldsymbol{r}_i)\,\mathrm{d}A_i - \sum_{i=1}^{N} \int_{A_i}\int_{A_i} \chi_i(\boldsymbol{r}_i)\chi_i(\boldsymbol{r}_i')K_{ii}(\boldsymbol{r}_i, \boldsymbol{r}_i')\,\mathrm{d}A_i\,\mathrm{d}A_i' - 2\sum_{j=2}^{N}\left[\sum_{i=1}^{j-1} \int_{A_i}\int_{A_j} \chi_i(\boldsymbol{r}_i)\chi_j(\boldsymbol{r}_j)K_{ij}(\boldsymbol{r}_i, \boldsymbol{r}_j)\,\mathrm{d}A_j\,\mathrm{d}A_i\right]. \quad (10)$$

It is possible to present the third and the fourth terms on the right-hand-side of equation (10) as one term using the symmetric property of K_{ij}. However, the third term is extracted to show the effect of the total irradiation from the surface i towards itself. Following the standard variational steps, the minimization of equation (10) leads to equation (9). This can be demonstrated by setting

$$\chi_k(\boldsymbol{r}_k) = \bar{\chi}_k(\boldsymbol{r}_k) + \omega_k\eta_k(\boldsymbol{r}_k) \quad (11)$$

for a surface k; $k = 1, 2, \ldots, N$. Notice that ω_k is a member of a set identified by, $\Omega = \{\omega_1, \omega_2, \ldots, \omega_N\}$ and $\Omega = 0$ implies that each member of the set is equal to zero. The extremum of this function is obtained when $(\partial I/\partial\omega_k)_{\Omega=0} = 0$ for $k = 1, 2, \ldots, N$. This leads to a relation [3],

$$\int_{A_k} \eta_k(\boldsymbol{r}_k)\left[\frac{1}{\lambda_k}\chi_k(\boldsymbol{r}_k) - \frac{1}{\lambda_k}\psi_k(\boldsymbol{r}_k) - \sum_{j=1}^{N} \int_{A_j} \chi_j(\boldsymbol{r}_j)K_{kj}(\boldsymbol{r}_k, \boldsymbol{r}_j)\,\mathrm{d}A_j\right]\mathrm{d}A_k = 0. \quad (12)$$

Recall that each $\bar{\chi}$ function becomes χ when $\Omega = 0$. Since equation (12) holds for all values of $\eta_k(\boldsymbol{r}_k)$, then the quan-

tity in the square brackets must have a zero value; therefore, the minimization of equation (10) yields equation (9). Of course, for this extremum to be a minimum, the second derivative of I with respect to ω_k must be positive. The second derivative is

$$\frac{\partial^2 I}{\partial \omega_k^2} = 2\left\{\frac{1}{\lambda_k}\int_{A_k}[\eta_k(\boldsymbol{r}_k)]^2\,\mathrm{d}A_k - \int_{A_k}\int_{A_k}\eta_k(\boldsymbol{r}_k)\eta_k(\boldsymbol{r}'_k)K_{kk}(\boldsymbol{r}_k,\boldsymbol{r}'_k)\,\mathrm{d}A'_k\,\mathrm{d}A_k\right\} \quad (13)$$

where prime indicates the dummy variable of integration for the inner integrals. Using the symmetric nature of K_{ij}, the second term in the braces, equation (13), is equal to,

$$\int_{A_k}\int_{A_k}\eta_k(\boldsymbol{r}_k)\eta_k(\boldsymbol{r}'_k)K_{kk}(\boldsymbol{r}_k,\boldsymbol{r}'_k)\,\mathrm{d}A'_k\,\mathrm{d}A_k = \int_{A_k}\int_{A_k}[\eta_k(\boldsymbol{r}'_k)]^2K_{kk}(\boldsymbol{r}_k,\boldsymbol{r}'_k)\,\mathrm{d}A'_k\,\mathrm{d}A_k - \frac{1}{2}\int_{A_k}\int_{A_k}[\eta_k(\boldsymbol{r}_k)-\eta_k(\boldsymbol{r}'_k)]^2K_{kk}(\boldsymbol{r}_k,\boldsymbol{r}'_k)\,\mathrm{d}A'_k\,\mathrm{d}A_k. \quad (14)$$

Combining equations (13) and (14) results in the relation

$$\frac{\partial^2 I}{\partial \omega_k^2} = 2\left\{\frac{1}{\lambda_k}\int_{A_k}[\eta_k(\boldsymbol{r}_k)]^2\,\mathrm{d}A_k - \int_{A_k}\int_{A_k}[\eta_k(\boldsymbol{r}'_k)]^2K_{kk}(\boldsymbol{r}_k,\boldsymbol{r}'_k)\,\mathrm{d}A'_k\,\mathrm{d}A_k\right\} + \int_{A_k}\int_{A_k}[\eta_k(\boldsymbol{r}_k)-\eta_k(\boldsymbol{r}'_k)]^2K_{kk}(\boldsymbol{r}_k,\boldsymbol{r}'_k)\,\mathrm{d}A'_k\,\mathrm{d}A_k > 0. \quad (15)$$

Since both terms on the right side of equation (15) are positive, the inequality holds. The function η_k is real and η_k^2 in equation (13) is always positive. The function η_k^2 can be regarded as an abstract radiosity of surface k. Because the integral

$$\int_{A_k}\int_{A_k}[\eta_k(\boldsymbol{r}'_k)]^2K_{kk}(\boldsymbol{r}_k,\boldsymbol{r}'_k)\,\mathrm{d}A'_k\,\mathrm{d}A_k$$

inside the brace, equation (15), represents a fraction of the abstract energy that the surface k irradiates on itself and the entire energy leaving surface k is

$$\int_{A_k}[\eta_k(\boldsymbol{r}_k)]^2\,\mathrm{d}A_k$$

therefore, the net value of the term in the curly brackets, equation (15), is positive, implying $\partial^2 I/\partial\omega_k^2 > 0$. Notice that when $I = -I$, equation (12) remains unchanged but in this case, $\partial^2 I/\partial\omega_k^2 < 0$; hence, only the extremum of function I is a sufficient condition to satisfy equations for energy interchange among surfaces.

3. Sparrow–Galerkin method

This method provides closed-form solutions to radiation exchange between surfaces. In ref. [3], it is proposed to replace $\chi_k(\boldsymbol{r}_k)$ in equation (10) by

$$\chi_k(\boldsymbol{r}_k) = \sum_{m=1}^{M} d_{k,m}f_{k,m}(\boldsymbol{r}_k) \quad (16)$$

for $i = 1, 2, \ldots, N$. After substitution, one must differentiate I with respect to $d_{k,m}$ to obtain a set of simultaneous equations. As an alternative procedure, one can substitute $\chi_k(\boldsymbol{r}_k)$ in equation (12) and obtain the same set of equations,

$$\int_{A_k} f_{k,n}(\boldsymbol{r}_k)\left[\frac{1}{\lambda_k}\sum_{m=1}^{M} d_{k,m}f_{k,m}(\boldsymbol{r}_k) - \frac{1}{\lambda_k}\psi_k(\boldsymbol{r}_k) - \sum_{j=1}^{N}\int_{A_j}\sum_{m=1}^{M} d_{j,m}f_{j,m}(\boldsymbol{r}_j)K_{kj}(\boldsymbol{r}_k,\boldsymbol{r}_j)\,\mathrm{d}A_j\right]\mathrm{d}A_k = 0 \quad (17)$$

for $k = 1, 2, \ldots, N$. Here, N is the total number of surfaces; however, M can vary from surface to surface. Equation (17) represents a set of $M \times N$ simultaneous algebraic equations. The solution of this set of equations,

$$\mathbf{A}\cdot\mathbf{d} = \psi \quad (18)$$

yields the coefficient in the set of $\mathbf{d} = \{\mathbf{d}_1, \mathbf{d}_2, \ldots, \mathbf{d}_N\}$, wherein every member of the kth subset has the elements $\mathbf{d}_k = \{d_{k,1}, d_{k,2}, \ldots, d_{k,M}\}$. The elements of the matrix $\mathbf{A}$ in equation (18) are

$$a_{m,n}^{k,j} = \frac{\delta_{kj}}{\lambda_k}\int_{A_k} f_{k,n}(\boldsymbol{r}_k)f_{j,m}(\boldsymbol{r}_k)\,\mathrm{d}A_k - \int_{A_k}\int_{A_j} f_{k,n}(\boldsymbol{r}_k)f_{j,m}(\boldsymbol{r}_k)K_{kj}(\boldsymbol{r}_k,\boldsymbol{r}_j)\,\mathrm{d}A_j\,\mathrm{d}A_k \quad (19)$$

where $\delta_{kj} = 1$ when $k = j$ and $\delta_{kj} = 0$ when $k \neq j$. For each pair of (k, j) $a_{m,n}^{k,j}$ describes a square matrix $\mathbf{A}^{k,j}$ whose locations in the square matrix $\mathbf{A}$ are shown below,

$$\mathbf{A} = \begin{bmatrix} \mathbf{A}^{1,1} & \mathbf{A}^{1,2} & \ldots & \mathbf{A}^{1,N} \\ \mathbf{A}^{2,1} & \mathbf{A}^{2,2} & \ldots & \mathbf{A}^{2,N} \\ \ldots & \ldots & \ldots & \ldots \\ \mathbf{A}^{N,1} & \mathbf{A}^{N,2} & \ldots & \mathbf{A}^{N,N} \end{bmatrix}. \quad (20a)$$

Each member of matrix $\mathbf{A}$ is an $M \times M$ matrix,

$$\mathbf{A}^{k,j} = \begin{bmatrix} a_{1,1}^{k,j} & a_{1,2}^{k,j} & \ldots & a_{1,M}^{k,j} \\ a_{2,1}^{k,j} & a_{2,2}^{k,j} & \ldots & a_{2,M}^{k,j} \\ \ldots & \ldots & \ldots & \ldots \\ a_{M,1}^{k,j} & a_{M,2}^{k,j} & \ldots & a_{M,M}^{k,j} \end{bmatrix} \quad (20b)$$

and satisfies the relation $\mathbf{A}^{j,k} = \mathbf{A}^{k,j}$, indicating the matrix $\mathbf{A}$ is symmetric. The array represented by $\psi = \{\psi_1, \psi_2, \ldots, \psi_N\}$ is a column vector that consists of subarrays, ψ_k. Each subarray ψ_k has the elements, $\psi_k = \{\psi_{k,1}, \psi_{k,2}, \ldots, \psi_{k,M}\}$, where

$$\psi_{k,m} = \int_{A_k}\frac{1}{\lambda_k}f_{k,m}(\boldsymbol{r}_k)\psi_k(\boldsymbol{r}_k)\,\mathrm{d}A_k. \quad (21)$$

Details concerning the computation of the radiosity using equations (16)–(20) are included in the following numerical example.

Example 1: This example concerns radiation exchange between two parallel circular disks, $N = 2$, whose numerical solution is available in the literature [14]. The centers of two circles are located on the same line and the line is perpendicular to both disks, see the inset in Fig. 2. Equation (12) for radiation exchange between these two disks with radii R_1 and R_2 is written as

$$\int_0^{R_1} \eta_1(r_1)\left[\frac{1}{1-\varepsilon_1}B_1(r_1) - \frac{1}{1-\varepsilon_1}\varepsilon_1\sigma T_1^4 - \int_0^{R_2} B_2(r_2)K_{12}(r_1,r_2)2\pi\,\mathrm{d}r_2\right]2\pi\,\mathrm{d}r_1 = 0 \quad (22a)$$

$$\int_0^{R_1} \eta_2(r_2)\left[\frac{1}{1-\varepsilon_2}B_2(r_2) - \frac{1}{1-\varepsilon_2}\varepsilon_2\sigma T_2^4 - \int_0^{R_1} B_1(r_1)K_{21}(r_2,r_1)2\pi\,\mathrm{d}r_1\right]2\pi\,\mathrm{d}r_2 = 0. \quad (22b)$$

In the standard Sparrow–Galerkin method, the radiosities, B_1 and B_2, are approximated using equation (16) where $f_{1,m}(r_1) = (r_1)^{2(m-1)}$ and $f_{2,m}(r_2) = (r_2)^{2(m-1)}$. Substitution of B_1 and B_2 in equations (22a) and (22b), and the assumption that $\eta_1 = f_{1,1}, f_{1,2}, \ldots, f_{1,M}$ and $\eta_2 = f_{2,1}, f_{2,2}, \ldots, f_{2,M}$, lead to $2M$ simultaneous equations described by equation (18).

The elements of matrix **A** and ψ were calculated using MATHEMATICA [15] and FORTRAN. Following matrix inversion, the values of $B_1/\sigma T_1^4$ (or $B_2/\sigma T_1^4$) for a test case, when $T_1 = T_2$, $R_1 = R_2 = 1$, $h = 0.5$, $\varepsilon_1 = \varepsilon_2 = 0.5$, are presented in Table 1. Table 2 contains the computed values of $B_1/\sigma T_1^4$ (or $B_2/\sigma T_1^4$) at various surface locations for $h/R_1 = 0.1$, 0.5, and 1.0 and for different values of emittance. For this example, convergence is achieved to five significant figures when $M = 7$. The error in the data is small for all M-values listed in Table 1; within 0.7% when $N = 2$. The calculation of the elements of matrix **A** requires numerical integration. The symbolic program MATHEMATICA produced $\mathbf{d}_1 = \mathbf{d}_2 = \{0.806105, -0.124519, -0.0960931, 0.0481751\}$. For the same task, a FORTRAN program used only a few seconds of computer time and produced the coefficients $\mathbf{d}_1 = \mathbf{d}_2 = \{0.806103, -0.124493, -0.0961565, 0.0482163\}$; about an order of magnitude faster. All computations were performed on a personal computer.

The Sparrow–Galerkin method, in general, converges rapidly to the exact values of $B_1/\sigma T_1^4$ and $B_2/\sigma T_1^4$, except when $B_1/\sigma T_1^4$ or $B_2/\sigma T_1^4$ is nearly flat over a section of the surface and its value changes rapidly over another section. Two graphs are presented to show the behavior of the Sparrow–Galerkin solution. Figure 2 shows the variation of $B_1/\sigma T_1^4$ (or $B_2/\sigma T_1^4$) vs. r_1/R_1 (or r_2/R_1) when $R_1 = R_2$, $h/R_1 = 0.1$, and $T_1 = T_2$. Despite the small dimension of the gap, the data are well behaved for $\varepsilon_1 = \varepsilon_2 = 0.1$ and 0.5. For the next case, the radius of the second disk is reduced to $R_2 = R_1/2$ while other variables remain the same as those in Fig. 2; that is $T_1 = T_2$, $h/R_1 = 0.1$, and $\varepsilon_1 = \varepsilon_2 = 0.1$ and 0.5. The values of $B_1/\sigma T_1^4$ and $B_2/\sigma T_1^4$ are plotted in Fig. 3. The value of $B_2/\sigma T_1^4$ is converging after a few terms while $B_1/\sigma T_1^4$ oscillates about the solution. The reason for these oscillations is that polynomials, even of degree 14 ($N = 8$), cannot adequately describe the changes in radiosity. There are two methods that overcome this difficulty. One method is to select a set of functions that have characteristics expected from the solution and is not discussed to avoid redundancy. The second, and simpler method, is to subdivide the surface into smaller surfaces and treat each as a different surface. The second scheme has a broader implication as it becomes the finite-element method. The finite-element technique is subject to certain approximations; each approximation is discussed in the next section.

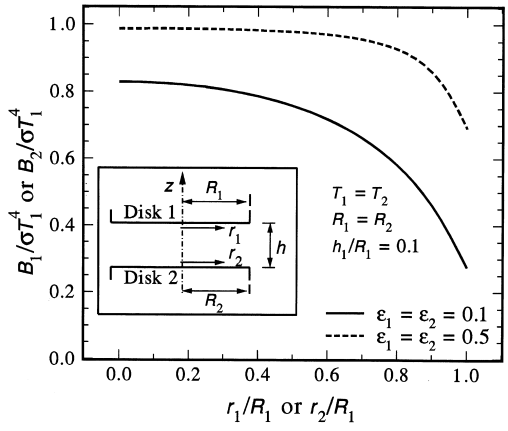

Fig. 2. Radiosity for two parallel disks when $T_1 = T_2$, $\varepsilon_1 = \varepsilon_2$, $R_2 = R_1$, and $h/R_1 = 0.1$.

4. Sparrow–Galerkin finite element

Sparrow's variational formulations are basic to the derivation of the finite-element procedure for computing the radiation interchange among surfaces. Formulation of the finite-element method of solution begins with equation (12). Each surface k is subdivided into M_k small surfaces and each is treated as a separate surface for inclusion in equation (12). The next step is to define χ and η functions for all elements. Similar to the standard finite-element procedure, the χ functions are described by linear functions of local coordinates for each of the elements, e.g.,

$$\chi_k(\xi_m, \zeta_m) = (1-\xi_m-\zeta_m)\chi_{k,m} + \xi_m\chi_{k,l} + \zeta_m\chi_{k,p} \quad (23)$$

where $\chi_{k,m}$, $\chi_{k,l}$, and $\chi_{k,p}$ are corner nodes for element m having coordinates $(0,0)$, $(1,0)$, and $(0,1)$, respectively,

Table 1
Radiosity $B_1/\varepsilon\sigma T_1^4$ (or $B_2/\varepsilon\sigma T_1^4$) when $T_1 = T_2$, $R_1 = R_2 = 1$, $h = 0.5$, and $\varepsilon_1 = \varepsilon_2 = 0.5$

r_1 or r_2	$M = 2$	$M = 3$	$M = 4$	$M = 5$	$M = 6$	$M = 7$	$M = 8$
0.0	0.81261	0.80855	0.80610	0.80659	0.80665	0.80662	0.80662
0.1	0.81083	0.80701	0.80485	0.80524	0.80529	0.80527	0.80527
0.2	0.80551	0.80237	0.80097	0.80114	0.80114	0.80115	0.80115
0.3	0.79663	0.79453	0.79415	0.79407	0.79405	0.79406	0.79406
0.4	0.78420	0.78336	0.78392	0.78371	0.78369	0.78370	0.78370
0.5	0.76823	0.76866	0.76972	0.76958	0.76959	0.76958	0.76958
0.6	0.74870	0.75018	0.75107	0.75112	0.75114	0.75114	0.75114
0.7	0.72563	0.72760	0.72769	0.72787	0.72787	0.72788	0.72788
0.8	0.69900	0.70055	0.69968	0.69973	0.69971	0.69971	0.69971
0.9	0.66882	0.66860	0.66780	0.66760	0.66761	0.66761	0.66761
1.0	0.63510	0.63129	0.63367	0.63415	0.63409	0.63406	0.63406

Table 2
The value of $B_1/\sigma T_1^4$ (or $B_2/\sigma T_1^4$) for different values of h and $\varepsilon_2 = \varepsilon_1$ when $M = 8$

h/R_1	r_1/R_1	$\varepsilon_1 = 0.1$	$\varepsilon_1 = 0.3$	$\varepsilon_1 = 0.5$	$\varepsilon_1 = 0.7$	$\varepsilon_1 = 0.9$
0.1	0.0	0.82861	0.96664	0.98757	0.99491	0.99868
	0.2	0.81931	0.96453	0.98742	0.99519	0.99885
	0.4	0.78591	0.95262	0.98269	0.99326	0.99835
	0.6	0.71767	0.92354	0.97093	0.98887	0.99737
	0.8	0.58088	0.83897	0.92748	0.96965	0.99251
	1.0	0.27473	0.52219	0.69069	0.82741	0.94572
0.5	0.0	0.28545	0.62405	0.80662	0.91284	0.97749
	0.2	0.28126	0.61754	0.80115	0.90948	0.97641
	0.4	0.26836	0.59715	0.78370	0.89852	0.97280
	0.6	0.24592	0.56043	0.75114	0.87733	0.96556
	0.8	0.21339	0.50485	0.69971	0.84241	0.95312
	1.0	0.17483	0.43641	0.63406	0.79629	0.93616
1.0	0.0	0.17065	0.44647	0.65678	0.81958	0.94691
	0.2	0.16913	0.44336	0.65351	0.81713	0.94597
	0.4	0.16462	0.43415	0.64380	0.89082	0.94314
	0.6	0.15741	0.41935	0.62813	0.79799	0.93855
	0.8	0.14817	0.40031	0.60785	0.78261	0.93255
	1.0	0.13807	0.37937	0.58547	0.76556	0.92586

in the local coordinate system (ξ_m, ζ_m). Accordingly, all integrations in equation (17) will have exact values, except those having the function K_{kj} in the integrand. A finite-element procedure requires a reasonably accurate evaluation of the integrals that include K_{kj} functions. Numerical integrations can be elaborate when the number of elements is large. Three approximations are selected for the calculation of K_{kj} between element m on surface k and element n on surface j.

(1) Integrals that include K_{kj} functions are numerically integrated.
(2) Assume $K_{kj}(\boldsymbol{r}_{k,m}, \boldsymbol{r}_{j,n})$ as a constant evaluated using $\boldsymbol{r}_{k,m}$ and $\boldsymbol{r}_{k,n}$ at the centeroids of the mth element on surface k, and the nth element on surface j.
(3) Calculate $K_{kj}(\boldsymbol{r}_{k,m}, \boldsymbol{r}_{j,n})$ using the coordinates of each of the nodal points of element m on surface k and nodal points of element n on surface j, then average the calculated $K_{kj}(\boldsymbol{r}_{k,m}, \boldsymbol{r}_{j,n})$ values.

The finite-element steps, and a discussion concerning the accuracy of the three approximations mentioned above are presented through a simple numerical examples.

Example 2: Equation (2) describes the radiation interchange between two parallel disks described in Example

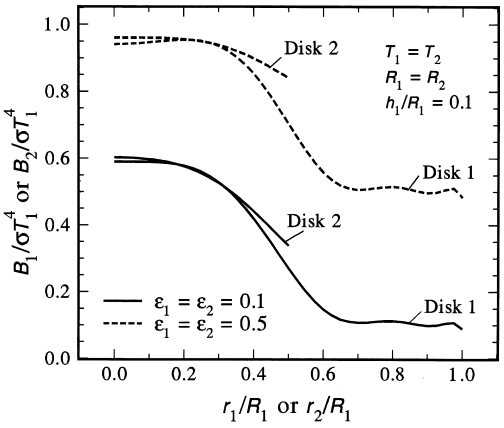

Fig. 3. Radiosity for two parallel disks when $T_1 = T_2$, $\varepsilon_1 = \varepsilon_2$, $R_2 = R_1/2$, and $h/R_1 = 0.1$.

1. Each of the parallel disks, 1 and 2, are subdivided into M_1 and M_2 elements, respectively, Fig. 4. The size of surface elements on Disks 1 and 2 are $\Delta r_1 = R_1/M_1$ and $\Delta r_2 = R_2/M_2$. The unknown function χ_k for $k = 1$ or 2, over the element m is

$$\chi_k = (1-\xi_{k,m})\chi_{k,m} + \xi_{k,m}\chi_{k,m+1}, \quad \text{for } r_{k,m} < r_k < r_{k,m+1} \tag{24}$$

when $\xi_{k,m} = (r_k - r_{k,m})/(r_{k,m+1} - r_{k,m})$ is the local coordinate that replaces r_k, and for elements m on surface k, see Fig. 4, where $r_{k,m+1} - r_{k,m} = \Delta r_{k,m}$. In this example, $\Delta r_{k,m} = \Delta r_k$ is a constant.

Substituting for χ_1 and χ_2, given by equation (24), into equation (10) yields a function $I(\chi_{1,m}, \chi_{2,m})$, for $m_1 = 1, 2, \ldots, M_1$ and $m_2 = 1, 2, \ldots, M_2$. Now, the polynomial coefficients $d_{k,m}$ in the Sparrow–Galerkin method are replaced by $\chi_{k,m}$. Based on the formulation presented earlier, one must set $\partial I/\partial \chi_{k,m} = 0$ for node m_k, Fig. 4, on surface k. This yields a simple relation that has the contribution of integrals over the elements adjacent to this node. The resulting equations in the matrix form are,

$$\mathbf{A} \cdot \chi = \psi. \tag{25}$$

Matrix **A** has a form similar to the matrix **A** in equation

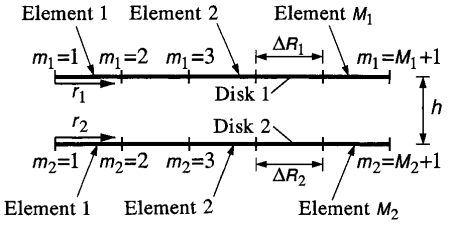

Fig. 4. Finite elements over two parallel disks.

(20a); however, the entries in equation (20a) are to be modified. To describe the formulation, let us consider each element as an independent surface. Equation (24) describes the variation of χ functions for each element where $(1-\xi_{k,m})$ and $\xi_{k,m}$ are the basis functions while $\chi_{k,m}$ and $\chi_{k,m+1}$ are the coefficients to be determined. Using the standard Sparrow–Galerkin method, there are two equations for each element. Solving this system should yield different values for $\chi_{k,m}$: one for element $m-1$ and the other for m. However, the number of equations in the finite-element method is less because the value of $\chi_{k,m}$ for elements m and $m-1$ must be identical. The formulation of the finite-element method requires considering equation (12) and treating each element as a separate surface with χ_k given by equation (24). For example, since $\chi_{k,m}$ is a constant to be determined, differentiating I with respect to $\chi_{k,m}$ yields the function η_k in equation (12). For adjacent elements, the contributions to η_k are from the basis functions $1-\xi_{k,m}$ of the node m and from the basis function $\xi_{k,m-1}$ of the node $m-1$, see equation (24). These two contributions are added since, in equation (12), $\chi_{k,m}$ has equal values for neighboring elements. For this specific example, matrix **A** consists of four square matrices, see equation (20a). The matrices $\mathbf{A}^{1,1}$ and $\mathbf{A}^{2,2}$ are tridiagonal since $K_{11} = K_{22} = 0$. Using the above procedure, each row, m, has contributions from element $m-1$ and element m so that

$$a^{k,k}_{m,m-1} = [\Delta r_k^2/12 + \Delta r_k r_{k,m-1}/6]/\lambda_k \tag{26a}$$

$$a^{k,k}_{m,m} = [(\Delta r_k^2/4 + \Delta r_k r_{k,m-1}/3) + (\Delta r_k^2/12 + \Delta r_k r_{k,m}/3)]/\lambda_k \tag{26b}$$

and

$$a^{k,k}_{m,m+1} = [\Delta r_k^2/12 + \Delta r_k r_{k,m}/6]/\lambda_k. \tag{26c}$$

The contribution of element $m-1$ to the diagonal term, $a^{k,k}_{m,m}$, is the term in the first parenthesis, equation (26b), while the term in the second parenthesis is the contribution of element m. Therefore, the first row of $\mathbf{A}^{k,k}$ only has the contribution of the first element and the last row (row M_k+1) has only the contribution from element M_k. The matrices $\mathbf{A}^{1,2}$ and $\mathbf{A}^{2,1}$ are full because $K_{12} = K_{21} \neq 0$. For each node, m, there are contributions from the neighboring elements, $m-1$ and m. According to equation (24), the value of the basis function for inclusion in equation (17) is $\xi_{k,m}$ for element $m-1$, and $1-\xi_{k,m}$ for element m. As before, for node 1, the contribution is from element 1, $\eta_{k,1} = 1-\xi_{k,1}$, and for node M_k+1, the contribution is from element m, $\eta_{k,m_k} = \xi_{k,m_k}$. The function χ_j in equation (17) must be integrated over all elements participating in thermal radiation; therefore, for this example, the matrices $\mathbf{A}^{1,2}$ and $\mathbf{A}^{2,1}$ are full and each entry has contributions from adjacent elements. The sum of the permuted contributions from adjacent elements yields the entry of matrices $\mathbf{A}^{1,2}$ and $\mathbf{A}^{2,1}$. For instance, $a^{k,j}_{m,n}$ has contributions from elements $m-1$ and m on the surface k, plus $n-1$ and n on surface j,

$$a_{m,n}^{k,j} = -\int_{r_{k,m-1}}^{r_{k,m}} \xi_{k,m-1}\left[\int_{r_{j,n-1}}^{r_{j,n}} (1-\xi_{j,n-1})K_{k,j}2\pi r_j\,\mathrm{d}r_j + \int_{r_{j,n}}^{r_{j,n+1}} \xi_{j,n-1}K_{k,j}2\pi r_j\,\mathrm{d}r_j\right] r_k\,\mathrm{d}r_k - \int_{r_{k,m-1}}^{r_{k,m}} (1-\xi_{k,m-1}) \times \left[\int_{r_{j,n-1}}^{r_{j,n}} (1-\xi_{j,n-1})K_{k,j}2\pi r_j\,\mathrm{d}r_j + \int_{r_{j,n}}^{r_{j,n+1}} \xi_{j,n-1}K_{k,j}2\pi r_j\,\mathrm{d}r_j\right] r_k\,\mathrm{d}r_k. \tag{27}$$

The nodes $m = 1$ and $m = M_k+1$ on surface k and nodes $n = 1$ and $n = M_j+1$ on surface j should receive special attention since each node is adjacent to only one element. Similarly, the members of the array ψ have contribution from elements adjacent to that member

$$\psi_{k,m} = \int_{r_{k,m-1}}^{r_{k,m}} \xi_{k,m-1}\frac{1}{\lambda_k}\psi_{k,m-1}r_k\,\mathrm{d}r_k + \int_{r_{k,m}}^{r_{k,m+1}} (1-\xi_{k,m})\frac{1}{\lambda_k}\psi_{k,m}r_k\,\mathrm{d}r_k \tag{28}$$

where the first term on the right-hand-side is the contribution of elements $m-1$; it is equal to $(\Delta r_k^2/3 + r_{k,m-1}\Delta r_k/2)\psi_k/\lambda_k$. Similarly, the contribution of the contribution of the element m is $(\Delta r_k^2/6 + r_{k,m}\Delta r_k/2)\psi_k/\lambda_k$. The sum of both terms in equation (28) is $r_{k,m}\Delta r_k\psi_k/\lambda_k$. For node 1, the contribution of element 1 is $\Delta r_k^2\psi_k/6\lambda_k$ while for $m = M_k+1$, only the contribution of the node $m-1 = M_k$ is used.

As a test case, the data in Table 1 are reproduced by the finite-element method. The data for the first approximation, where the kernel function, K_{ij} is position dependent, are produced by numerical integration of integrals in equation (27). For $M_1 = M_2 = 10$ and 20, the data in Table 3 show a remarkably high degree of accuracy. The second approximation produces larger errors observed mainly at end points. This approximation is easier to implement numerically. A variation of this, not presented here, is to calculate the K_{kj} function using the arithmetic mean of coordinates of the nodal points surrounding each element. This resulted in slightly larger errors than the second approximation data. Approximation 3 is easiest to implement; however, it provided slightly larger errors.

A remarkable feature of the finite-element method is demonstrated by repeating the calculations presented in Fig. 3 for two disks of different radii. The finite-element method effectively deals with variation of radiosities over both surfaces. Figure 5a is for $R_2 = R_1/2$ and $\varepsilon = \varepsilon_1 = \varepsilon_2 = 0.1$, and two different h/R_1 values. Unlike the data in Fig. 3, there are no visible oscillations and the data for the finite-element method, using the first approximation, are quite smooth. For the second approximation, there is a small error in the value of radiosity at $r_1 = 0$ only when $h/R_1 = 0.1$. Figure 5b is for the same variables as Fig. 5a, except the emittance for both surfaces is 0.5. The higher emittance in Fig. 5b did not alter the behavior of the two solutions. This shows that for larger values of h/L, the approximations listed earlier are satisfactory. When the emittance suffers adverse localized changes, a finite element that numerically integrates over elements yields more accurate results. In fact, the data shown in Figs 5a and b were verified using a refined numerical evaluation and they showed excellent accuracy. The largest error observed in Fig. 5a is at $r = 0$ for both disks; 0.01% for the first approximation and 1.4% for the second approximation.

5. Comments

It is appropriate to describe a method for calculating K_{ij} for any pair of elements on i and j surfaces. A schematic of this pair of elements is given in Fig. 6. With any standard grid generation technique, all elements and their corresponding nodal coordinates are known. Because the finite-element technique is well established, the discussion presents the basic changes without exhaustive details. Much of the procedure is identical to the finite element formulations for solving various differential equations.

Equation (12) serves as the basic relation for the finite-element formulations. The finite element is instrumental in finding approximate radiosity distributions that minimize function I. According to the data in Figs 5a and b, numerical quadrature (first approximation) may become necessary when the spacing between participating surfaces is small. Otherwise, any approximate method of determining K_{ij} should provide data with sufficient accuracy. Once the elements on each surface are specified, one can define relations between local and global coordinates; local coordinates for the radiosity, equation (23) and the global coordinate for K_{ij}. After completion of the solution, one can express the radiosity in terms of global coordinates.

The generalized procedure to evaluate the kernel function K_{ij} for a pair of nodes on the surfaces A_i and A_j is as follows. The function

$$K_{ij} = \frac{\cos\beta_i\cos\beta_j}{r_{ij}^2}$$

depends on local quantities that can be defined as follows. The variable r_{ij} is a distance between a point (x_i, y_i, z_i) on surface A_i and a point (x_j, y_j, z_j) on surface A_j. It is the magnitude of the vector

$$\boldsymbol{r}_{ij} = (x_j-x_i)\boldsymbol{i} + (y_j-y_i)\boldsymbol{j} + (z_j-z_i)\boldsymbol{k}$$

where $\boldsymbol{i}, \boldsymbol{j}, \boldsymbol{k}$ are unit vectors along x, y, and z coordinates. The unit vector along $\boldsymbol{r}_{ij}$, point toward surface A_j, is

Table 3
Raidosity $B_1/\varepsilon\sigma T_1^4$ (or $B_2/\varepsilon\sigma T_1^4$) when $T_1 = T_2$, $R_1 = R_2 = 1$, $h = 0.5$, $\varepsilon_1 = \varepsilon_2 = 0.5$, and $M_1 = M_2 = M$

r_1 or r_2	Finite element approx. 1		Finite element approx. 1		Finite element approx. 2		Finite element approx. 3		Table 1
	$M = 10$	Error %	$M = 20$	Error %	$M = 20$	Error %	$M = 20$	Error %	$M = 8$
0.0	0.80695	0.044	0.80670	0.010	0.80633	0.035	0.80785	0.152	0.80662
0.1	0.80548	0.026	0.80532	0.006	0.80490	0.046	0.80625	0.122	0.80527
0.2	0.80139	0.030	0.80121	0.007	0.80085	0.037	0.80186	0.089	0.80115
0.3	0.79434	0.935	0.79413	0.009	0.79385	0.026	0.79447	0.052	0.79406
0.4	0.78401	0.040	0.78377	0.009	0.78356	0.018	0.78382	0.015	0.78370
0.5	0.76994	0.047	0.76967	0.012	0.76952	0.008	0.76949	0.012	0.76958
0.6	0.75155	0.055	0.75124	0.013	0.75114	0.000	0.75090	0.032	0.75114
0.7	0.72830	0.058	0.72798	0.014	0.72793	0.007	0.72755	0.045	0.72788
0.8	0.70006	0.050	0.69980	0.013	0.69980	0.013	0.69940	0.044	0.69971
0.9	0.66771	0.015	0.66764	0.004	0.66802	0.061	0.66772	0.016	0.66761
1.0	0.63396	0.016	0.63403	0.016	0.63892	0.766	0.63881	0.749	0.63406

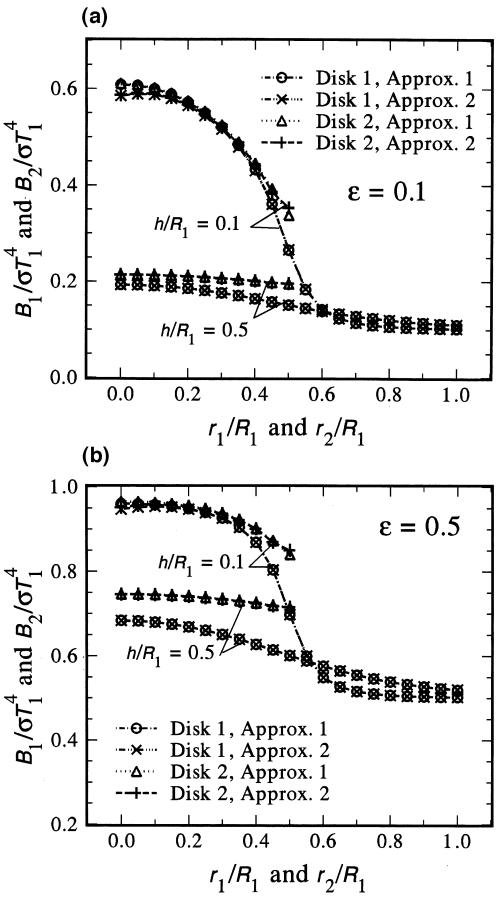

Fig. 5. (a) Radiosity for two parallel disks when $R_2 = R_1/2$, $T_1 = T_2$, $\varepsilon = \varepsilon_1 = \varepsilon_2 = 0.1$, and $h/R_1 = 0.1$ and 0.5 by finite element method (approximation 1). (b) Radiosity for two parallel disks when $R_2 = R_1/2$, $T_1 = T_2$, $\varepsilon = \varepsilon_1 = \varepsilon_2 = 0.5$, and $h/R_1 = 0.1$ and 0.5 by finite element method (approximation 1).

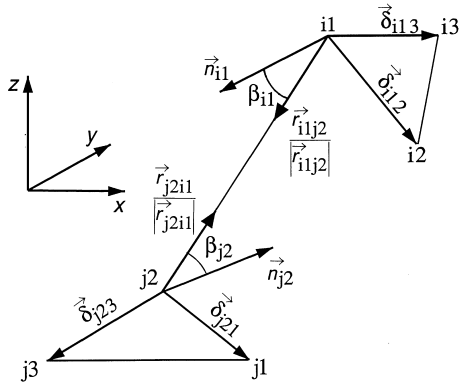

Fig. 6. Schematic of two elements i and j for calculation of k_{ij}.

$$\frac{\boldsymbol{r}_{ij}}{|\boldsymbol{r}_{ij}|}.$$

For example, using node 1 on the surface A_i and node 2 on surface A_j in Fig. 6, this unit vector becomes

$$\frac{\boldsymbol{r}_{i1j2}}{|\boldsymbol{r}_{i1j2}|}.$$

If $\boldsymbol{n}_{i1}$ is the unit vector normal to surface A_i at the nodal point 1, then $\cos\beta_i$ is

$$\cos\beta_i = \boldsymbol{n}_{i1} \cdot \left(\frac{\boldsymbol{r}_{i1j2}}{|\boldsymbol{r}_{i1j2}|}\right)$$

where

$$\boldsymbol{n}_{i1} = \frac{\delta_{i12} \times \delta_{i13}}{|\delta_{i12} \times \delta_{i13}|}$$

$$\delta_{i12} = (x_{i2} - x_{i1})\boldsymbol{i} + (y_{i2} - y_{i1})\boldsymbol{j} + (z_{i2} - z_{i1})\boldsymbol{k}$$

and

$$\delta_{i12} = (x_{i3} - x_{i1})\boldsymbol{i} + (y_{i3} - y_{i1})\boldsymbol{j} + (z_{i3} - z_{i1})\boldsymbol{k}.$$

A similar procedure applies for determination of $\cos\beta_j$. For the example used earlier, $\cos\beta_i$ and $\cos\beta_j$ are equal; however, in general, they are not the same for any pair of nodal points on surfaces A_i and A_j. The deviations given above for the calculation of angle factors equally apply to surface elements of different shapes.

6. Conclusions

It was shown that equation (17) will formally replace equation (5) derived by Sparrow [1] and equation (10) by Sparrow and Haji-Sheikh [3]. Alternatively, the Galerkin method developed to solve differential equations, if applied to equation (9), yields equation (17). For this reason, it is appropriate to reiterate that the solution of a set of integral equations described by equation (9) is designated as the Sparrow–Galerkin method. Here, it is shown that both methods lead to an identical set of equations and the Sparrow–Galerkin method satisfies the Ritz variational principles and paves the way toward a better understanding of the finite-element method. Dividing each surface into smaller surfaces, the Sparrow–Galerkin method leads to the standard finite element formulation. The higher-order finite element, the *p*-method, is also a direct and automatic extension of the Sparrow–Galerkin method.

The work reported by Sparrow [1] represents the pioneering step for development of powerful solution techniques to compute radiation exchange between surfaces. The Sparrow–Galerkin method and Sparrow–Galerkin-based, finite-element method are based on variational principles developed by Sparrow [1, 3]. Both methods are powerful and useful solution techniques that are currently in use. The presentation in this paper is for linear systems. When thermal radiation takes place in conjunction with conduction or convection, the governing integral equations are nonlinear. One can modify the finite element formulation for solving these nonlinear systems. For solving nonlinear integral or integrodifferential equations, one must develop a linearization scheme but this is beyond the scope of this presentation.

References

[1] E.M. Sparrow, Application of variational methods to radiation heat-transfer calculations, Journal of Heat Transfer, Transactions of ASME, Series C 82 (4) (1960) 375–380.

[2] L.V. Kantorovich, V.I. Krylov, Approximate Methods of Higher Analysis, Interscience Publishers, New York, N.Y., 1958.

[3] E.M. Sparrow, A. Haji-Sheikh, A generalized variational method for calculating radiant interchange between surfaces, Journal of Heat Transfer, Transactions of ASME, Series C, 87 (1) (1965) 103–109.

[4] K.H. Huebner, E.A. Thornton, T.G. Byrom, The Finite Element Method for Engineers, 3rd ed., John Wiley and Sons, New York, 1995.

[5] J.V. Daurelle, R. Occelli, R. Martin, Finite-element modeling of radiation heat transfer coupled with conduction in an adaptive method, Numerical Heat Transfer, Part B: Fundamentals 25 (1994) 61–73.

[6] M. Lobo, A.F. Emery, The use of discrete maximum principle in finite element analysis of combined conduction and radiation in nonparticipating media, ASME HTD 257 (1993) 11–23.

[7] M. Lobo, A.F. Emergy, The discrete maximum principle in finite element thermal radiation analysis, Numerical Heat Transfer, Part B—Fundamentals, 24 (1993) 209–227.

[8] S. Kuppurao, J.J. Derby, Finite-element formulations for accurate calculation of radiant heat transfer in diffuse-gray enclosures, Numerical Heat Transfer, Part B—Fundamentals 24 (3) (1993) 431–454.

[9] A. Sanchez, T.F. Smith, Surface radiation exchange for two-dimensional rectangular enclosures using the discrete-ordinate method, ASME Journal of Heat Transfer 114 (2) (1992) 465–472.

[10] W.A. Fiveland, The selection of discrete ordinate quadrature sets for anisotropic scattering, ASME HTD 160 (1991) 89–96.

[11] W.A. Fiveland, J.P. Jessee, Finite element formulation of the discrete ordinate method for multidimensional geometries, Journal of Thermophysics and Heat Transfer, 8 (3) (1994) 426–433.

[12] D.A. Kaminski, X.D. Fu, M.K. Jensen, Numerical and experimental analysis of combined convective and radiative heat transfer in laminar flow over a circular cylinder, International Journal of Heat and Mass Transfer 38 (17) (1995) 3161–3169.

[13] S.P. Burns, J.R. Howell, D.E. Klein, Empirical evaluation of an important approximation for combined-mode heat transfer in a participating medium using the finite element method, Numerical Heat Transfer, Part B—Fundamentals 27 (3) (1995) 309–322.

[14] E.M. Sparrow, J.L. Gregg, Radiant interchange between circular disks having arbitrary different temperature, Journal of Heat Transfer, Transactions of ASME, Series C 83 (4) (1961) 494–502.

[15] S. Wolfram, The Mathematica Book, Cambridge University Press, 1996.